Acta Astronautica. Vol. 3, pp. 795–810. Pergamon Press 1976. Printed in the U.S.A.

Detonation and critical diameter of heterogeneous explosives†

ROBERT F. CHAIKEN AND JOHN C. EDWARDS

Pittsburgh Mining and Safety Research Center, Bureau of Mines, U.S. Department of the Interior, Pittsburgh, Penn., U.S.A.

(*Received* 14 *July* 1975; *revised* 4 *December* 1975)

Abstract—A kinetic lattice model of heterogeneous detonation reaction is developed which treats localized ignition and grain burning as an integral part of the detonation reaction, and which allows the reaction time to be defined in terms of a large set of competing reaction rates, defined for all the components of an explosive mixture. Coupling the lattice reaction rate equations to hydrothermodynamic equations for non-ideal detonation defines an initial value problem which describes the region of stable detonation. Numerical solution of the problem in velocity-density space leads to a determination of the critical diameter of the explosive as well as to a determination of physical and/or chemical parameters (e.g. loading density and particle size) that can yield nonstable detonations. Examples are shown that predict the explosive group behavior described by Price and the critical diameters for several types of explosive materials.

Introduction

IT HAS long been recognized that the physical character of a granular explosive (e.g. particle size, porosity, loading density and confinement) contributes to determining the detonability of the explosive.‡ This is particularly true in the non-ideal region of detonation (i.e. small diameter charges) where energy loss by side expansion removes energy from the chemical reaction zone supporting the detonation front. Defining the detonation reaction zone or reaction time in heterogeneous explosives is thus important for predicting this energy loss and for determining the detonation stability criteria.

Eyring *et al.* (1949) in their classical "grain burning" theory suggested that for granular explosives, the detonation reaction time, τ, can be expressed as,

$$\tau = \bar{R}_g / \lambda k_r \tag{1}$$

where $\bar{R}_g$ is the average radius of the granules, λ is the thickness of an explosive monolayer, and $(k_r)^{-1}$ is the effective lifetime of an explosive molecule.

This expression implicitly assumes that ignition of grain burning occurs instantaneously (e.g. via hot-spot formation) at the surface of each particle after passage of the detonation front. However, under certain conditions of porosity, packing geometry and/or shock strength, it is conceivable that the time to ignition, the amount of explosive involved in the ignition, and the effective distance between ignition sites may be a significant part of the total detonation reaction.

†Paper presented at the Fifth Colloquium on Gasdynamics of Explosions and Reactive Systems, Bourges, France, 8–11 September 1975.

‡See Taylor (1952), Cook (1958) and Johansson and Persson (1970).

For heterogeneous explosives with finite ignition times, the detonation behavior would be much more complex than that depicted by eqn (1).

It is the purpose of this paper to describe a kinetic lattice model of heterogeneous detonation reaction which treats ignition as an integral part of the detonation reaction zone and to demonstrate how, in this circumstance, competing reaction rates can affect the non-ideal detonation behavior of the explosive. A somewhat simplistic set of hydrodynamic coupling equations are used for this latter purpose, which somewhat limits the accuracy of the calculated detonation parameters. However, the approach taken does lead to an explanation of some of the more unusual observed detonation phenomena with granular explosives, such as the Group I/Group II behavior described by Price (1967).

One-dimensional kinetic lattice model

A heterogeneous explosive is taken to be a lattice network, composed of uniformly distributed initiation sites (e.g. particles, voids, contact surfaces, defects, etc.), each having a finite volume. When a detonation front overtakes a region in the explosive, the initiating sites begin to react, forming hot-spots. The formation of a hot-spot is accompanied (with zero delay) by a burning reaction growing from the hot-spot, consuming initiating sites (i.e. explosive) as the burning front spreads. Complete reaction of the lattice network defines the end of the detonation reaction zone.

In the present one-dimensional treatment of the lattice model, the burning reaction rate is assumed to be described by a linear velocity, B. The initiating sites may be of different types (subscript i), characterized by a length L_i and a reaction rate constant k_i. The lattice at any time t from the instant of passage of the detonation front will consist of $N_i(t)$ initiating sites of type i and $N_T^*(t) = \Sigma N_i^*(t)$ total hot-spots.

A schematic representation of the 1-D lattice is shown in Fig. 1.

Assuming hot-spot formation to be a first order process, the rate of formation of hot-spots N_i^* is given by

$$dN_i^*/dt = k_i N_i. \tag{2}$$

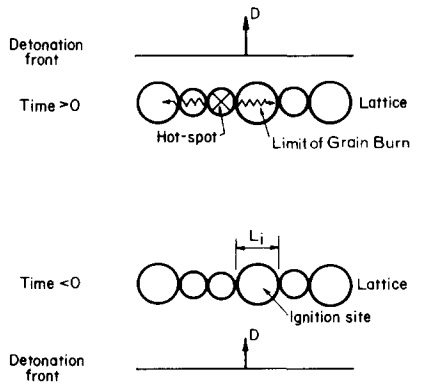

Fig. 1. Schematic representation of a lattice model of detonation.

The rate of decrease of N_i is then given by

$$-\frac{dN_i}{dt} = k_i N_i + \frac{2BN_T^* N_i}{\Sigma_j L_j N_j}, \quad j = 1, 2, \ldots \tag{3}$$

where $N_T^* = \Sigma N_i^*$.

The first term in eqn (3) is simply the first order activation process to form hot-spots, while the second term is the rate of combustion of initiating sites by the burning reaction. The form of the second term may be more readily seen by noting that $\Sigma L_j N_j / N_T^*$ is the average distance between hot-spots at any time. The burning time between hot-spots (with the burning front spreading in two directions) is then

$$\tau_b = \frac{\Sigma L_j N_j / N_T^*}{2B}. \tag{4}$$

Since $(\tau_b)^{-1}$ is an effective first order burning rate constant

$$-\left.\frac{dN_i}{dt}\right|_{\text{burning}} = \frac{2BN_T^* N_i}{\Sigma L_j N_j}. \tag{5}$$

It is noted that eqn (4) leads directly to the Eyring grain-burning expression (eqn 1) when we have a single type site ($i = 1$) and instantaneous hot-spot formation (i.e. $N_T^* = N_i$). In this case, the linear burning rate is taken as $B = \lambda k_r$.

Equations (2) and (3) represent the rate of disappearance of explosive. They are nonlinear and require numerical solution.

In utilizing the lattice model to determine detonation reaction times, the rate constants k_i and burning rate B would normally depend upon temperature in the detonation zone (Andersen and Chaiken, 1959; 1961), i.e.

$$k_i = A_i \exp(-E_i/RT)\ \text{sec}^{-1} \tag{6}$$

$$B = A_s \exp(-E_s/RT)\ \text{cm/sec} \tag{7}$$

where the A's and E's are Arrhenius constants, R is the universal gas constant and T is the temperature at which the reaction is occurring. The value of the reaction temperature to be employed in the Arrhenius rate constant expressions poses a considerable problem. Several real factors should be considered in this connection: (1) non uniform shock heating by the detonation front; (2) non uniform self heating due to local decomposition reactions; and (3) temperature increasing with time due to progression of reaction. Since temperature effects the reaction rate constant primarily through the activation energy term E/RT, it is possible in the 1-D lattice model to consider a uniform lattice temperature at any instant in time, and to account for non uniform heating effects through the choice of activation energy for each type of site. However, a time dependent temperature through the detonation zone requires a coupling of the extent of reaction and the extent of self-heating which occurs, e.g.

$$T = T_{in} + \epsilon Q/C_v \tag{8}$$

where ϵ is the extent of reaction, Q is the specific heat of reaction, and T_{in} is some initial temperature at the detonation front.

For homogeneous explosives, it has been argued (Evans, 1962) that the time for complete reaction is defined primarily by the initial shock temperature, T_{sh}, through the usual Frank–Kamenetskii explosion time, i.e.

$$\tau_{\epsilon=1} = (\bar{C}_v RT_{sh}^2/AEQ) \exp(E/RT_{sh}), \tag{9}$$

which assumes an effective induction time for reaction. However, as pointed out in the detailed calculations of Petrone (1966) and Mader (1965) the effects of coupling the hydrodynamic steady-state detonation equations with finite reaction kinetics throughout the detonation reaction zone leads to temperature–time (or temperature–distance) profiles considerably different from that implied by eqn (9).

For a grain-burning reaction during steady-state detonation, the case against eqn (9) is even more valid since the reaction spreads in a layer-wise fashion as a wave from initiation centers (or hot-spots). In accordance with solid burning theories, the reaction temperature driving this wave will be close to the adiabatic flame temperature of the reacting material, which would have values closer to the Chapman–Jouguet temperature of the explosive than to the initiating shock temperature. For the purposes of this paper, which deals with steady-state detonations, we assume that the reaction temperature of each site can be identified with the Chapman–Jouguet temperature. This assumption, which was originally used by Eyring *et al.* (1949) in his failure theory greatly simplifies coupling between the kinetic lattice equations and the hydrodynamic expressions defining steady-state detonation, and at the same time, probably more closely approximates the actual complex temperature-time-space distributions that actually exist in the detonation reaction zone of heterogeneous explosives.

Hydrodynamic coupling relationships

The approach taken here is to couple the kinetic lattice reaction rate with the one dimensional hydrodynamic equations of Chapman–Jouguet (C–J) theory. A volume dependent covolume equation of state due to Cook (1958) is used to describe the P-V-T relationship for the detonation products which are treated as a single gas component.

The appropriate hydrothermodynamic relationships for the C–J state, where the pressure is much larger than in the initial state (i.e. $P \gg P_0$), can be written as†

mass/momentum conservation:

$$D^2 = \frac{P}{\rho_0(1 - \rho_0/\rho)} \tag{10}$$

momentum conservation:

$$u = P/(\rho_0 D) \tag{11}$$

†see Cook (1958), Johansson and Persson (1970) and Eyring *et al.* (1949).

energy conservation:

$$\Delta E = q_d + \frac{P(\rho - \rho_0)}{2\rho_0\rho} \tag{12}$$

Chapman–Jouguet condition:

$$c = D - u \tag{13}$$

equation of state:

$$P[1/\rho - \alpha(\rho)] = C_v(\gamma - 1)T \tag{14}$$

$$\alpha(\rho) = (1 - e^{b\rho})/\rho \tag{15}$$

where D is the detonation velocity; P, the pressure; ρ, the density; u, the particle velocity; ΔE, the change in specific internal energy; q_d, the heat of detonation; c, the local sound velocity $= (\partial P/\partial\rho)_s^{+1/2}$; C_v, an averaged constant volume heat capacity; γ, an averaged constant ratio of heat capacities $= C_p/C_v$; T, the absolute temperature; $\alpha(\rho)$, the density dependent covolume; and b, a constant equal to -1 cm^3/g. The subscript 0 refers to the initial state conditions of the explosive.

These equations yield the following expressions for the Chapman–Jouguet state variables:

$$P = \frac{2Q\rho_0\rho(\gamma - 1)}{2\rho_0(1 - \alpha\rho) - (\gamma - 1)(\rho - \rho_0)} \tag{16}$$

$$T = \frac{2\rho_0(1 - \alpha\rho)Q/C_v}{2\rho_0(1 - \alpha\rho) - (\gamma - 1)(\rho - \rho_0)} \tag{17}$$

$$\rho_0/\rho = \frac{\gamma}{1 - \alpha\rho}(1 + \rho^2\, d\alpha/d\rho)(1 - \rho_0/\rho) \tag{18}$$

where Q has been written for $q_d + C_vT_0$, and $\Delta E = C_vT - C_vT_0$.

To account for the effect of lateral rarefaction on energy loss from the detonation reaction zone, we employ the results of the Eyring curved front theory (Eyring *et al.*, 1949) which for uncased cylindrical charges yields the following simple expression for the diameter effect:

$$D/D_i = 1 - a/d \tag{19}$$

where a is the reaction zone length; d is the charge diameter; and D_i is the ideal detonation velocity determined by 1-D Chapman–Jouguet theory, e.g. by setting q_d to be the ideal heat of detonation $(q_d)_i$.

Noting that the length of the reaction zone is given by the product of the reaction time τ, and the relative particle velocity, $D - u$ in the reaction zone, we can write

$$D/D_i = 1 - \tau(D - u)/d, \tag{20}$$

and from eqn (11)

$$D^2(1/D_i + \tau/d) - D - \tau P/\rho_0 d = 0. \tag{21}$$

Equations (10)–(21) define the stable detonation wave (or absence of a stable wave) for any given reaction time.

A complete solution for D can now be obtained by defining τ through the kinetic lattice model expressions. In this case, the detonation temperature as determined from eqn (17) establishes the reaction rate constants as given in eqns (6) and (7) for all the lattice components.

In solving the equations for detonation velocity, Q is used as a stepping parameter to define a hydrodynamic τ and T (eqns 10, 17, 18 and 21). A kinetic τ (eqns 2 and 3) is then determined for these same sets of parameters.† The entire process is repeated for various Q until the hydrodynamic and kinetic τ values converge.

Before proceeding to the numerical examples, it is interesting to examine eqn (21) in some further detail. Expressing P as a function of D (eqns 10 and 18), we obtain from eqn (21)

$$\theta\left[1+\frac{\phi\tau}{d}\right]-1=0 \tag{22}$$

where $\phi=(\gamma\beta+\alpha\rho_0)D_i/(\gamma\beta+1)$

$\beta=1+\rho^2(\mathrm{d}\alpha/\mathrm{d}\rho)$

$\theta=D/D_i$.

$\tau(T)$ is some function of θ which when introduced into the above equation, will give a unique solution for θ. It is useful to examine the nature of those solutions for simple forms of the $\tau(\theta)$ dependence chosen *ad hoc*, viz. $\tau=A\theta^{-n}$ with $n\geq 1$.

This leads to

$$\theta\left[1+\frac{\phi A}{\theta^n d}\right]^{-1}=0 \tag{23}$$

or

$$\theta=1-\frac{\phi A}{d}, \quad \text{for } n=1 \tag{24}$$

and

$$\theta=\left[\frac{\phi A/d}{1-\theta}\right]^{1/(n-1)}, \quad \text{for } n>1. \tag{25}$$

The case for $n=1$ yields only a single solution for θ, but for $n>1$ we can obtain 0, 1 or 2 distinct real positive solutions.

Thus, we see that depending upon the kinetic $\tau(D)$ dependence, single or double solutions for D arise from this treatment. This was noted by both Eyring *et al.* (1949) and Evans (1962), who likewise utilized eqn (19) to express the diameter effect.

†The kinetic τ is determined by solving the ordinary differential equations by a Runge–Kutta method. In the solution process, whenever one of the N_i becomes less than unity, that particular N_i is set equal to zero for the remainder of the calculation. When all $N_i<1$, the corresponding time is taken as the kinetic τ.

Lattice construction

Prior to carrying out a solution of the lattice model, it is necessary to input the initial number of sites which relate to a specific explosive composition. These sites may consist of granules of solid explosive components, air spaces, crystal defects, contact surfaces, etc. By considering each site to be spherical in shape with a specified diameter L_i, and specified local density ρ_i (e.g. crystal density in the case of a solid granule), we can write two general relationships for the charge diameter and loading density ρ_0 in terms of the i sites, i.e.

$$d = \Sigma L_i N_i(0) \tag{26}$$

$$\rho_0 = \frac{\Sigma(1/6)\pi L_i^3 N_i(0)\rho_i}{\Sigma(1/6)\pi L_i^3 N_i(0)}. \tag{27}$$

If there are more than two types of sites, say n, then it requires $n-2$ other independent specifications to completely determine the $N_i(0)$'s. The volume and/or mass fraction of explosive components will suffice, or simply the value of $N_i(0)$ itself (which would probably have to be the case when defect or contact surface sites are considered).

When dealing with mass fractions, it is convenient to note the following simple relationship:

$$f_i = \frac{L_i^3 N_i(0)\rho_i}{\Sigma L_i^3 N_i(0)\rho_i}. \tag{28}$$

For the case of a porous granular solid, it is reasonable to identify the L_i of the granules with the average diameter of the explosive particles. The L_i for the air voids would require some consideration of the particle packing arrangement and effective size of the interstitial spaces. Crystal defect and contact surface sites would be somewhat complex, perhaps requiring a size specification on the order of molecular dimensions.

Numerical results and discussion

Several examples are chosen here to describe the applications of the theoretical approach. The first case to be discussed, involves a two component porous granular explosive where the detonation exhibits the contrasting explosive behavior patterns which were described by Price (1967). This example is used as a model to determine the effect of chemical and physical parameter variations on detonability.

In the next two cases discussed, an attempt is made with varying degrees of success to correlate experimental critical diameter data for specific explosive systems—a porous amatol mixture and an RDX modified composite propellant.

Case 1. *A two component porous granular explosive*

In constructing the lattice, the initiating sites are taken to be the individual granules of explosive ($i = 1$) and the air spaces between the granules ($i = 2$). For

simplicity the diameter of the two types of sites are considered equal (i.e. $L_1 = L_2 = L$), which leads directly to

$$N_i(0) = \frac{d}{L}\left[\frac{\rho_0 - \rho_2}{\rho_1 - \rho_2}\right] \tag{29}$$

$$N_2(0) = \frac{d}{L}\left[\frac{\rho_1 - \rho_0}{\rho_1 - \rho_2}\right]. \tag{30}$$

A temperature independent rate constant is assumed for the air sites. This is believed to be reasonable since shock heating of the air leads to very high temperatures, probably within the thickness of the shock front itself (defined by about 10^3 molecular vibrations).

The values of all the input parameters are shown in Table 1. It is noted that k_1 and B are not too different from rate constants reported for ammonium nitrate while the heat of detonation is somewhat higher than that of ammonium nitrate.

Figure 2 depicts the calculated results for $D(\rho_0)$ at various charge diameters. It is evident that the computed values of velocity are somewhat high, particularly at large ρ_0, which undoubtedly reflects on our use of the Cook equation of state with a constant heat of detonation. What is believed to be significant however, is the limited regions of detonation which occur at small charge diameters. The apex of the parabolic shaped curves for $d \leq 5.8$ cm apparently defines a critical diameter condition for detonation. When the calculated C–J pressures and reaction times for various ρ_0 are plotted in the $P - \tau$ plane, it appears that the pressure is an extremum at the apex point. If this is exactly the case, it is easily shown that such a constraint (i.e. $dP/d\tau = 0$) leads to a trivial solution of the detonation equations, i.e. $D = c = u = 0$. This indicates that there are no physically real solutions for which $dP/d\tau = 0$, and thus the apex point would indeed represent a failure point for the explosive. It is evident from Fig. 2 that there is no failure point for $d \geq 6.2$ cm.

It is also seen from Fig. 2 that the locus of failure points (dashed line) defines two velocity regimes of detonation. That is for every $d > d_{cr}$, two C–J detonation velocities can occur. As was discussed earlier, this arises from the Eyring failure theory with finite reaction kinetics. The higher velocity regime (where D

Table 1. Input parameters for Case 1 explosive

$\rho_1 = 1.725$ g/cm^3	$C_v = 0.4$ cal/g°K
$\rho_2 = 1.176 \times 10^{-3}$ g/cm^3	$\gamma = 1.5$
$L_1 = L_2 = 5 \times 10^{-3}$ cm	$(q_d)_i = 879$ cal/g
(a) $k_1 = 5.56 \times 10^9 \exp(-40{,}000/RT)$ sec^{-1}	
$k_2 = 5 \times 10^{10}$ sec^{-1}	$T_0 = 300$°K
(b) $B = 300 \exp(-7100/RT)$ cm/sec	

(a) Andersen and Chaiken (1959) cites $k = 10^{12.28} \exp(-38{,}300/RT)$ sec^{-1} for NH_4NO_3.

(b) Andersen and Chaiken (1959) cites $B = 0.23T \exp(-7100/RT)$ cm/sec for NH_4NO_3.

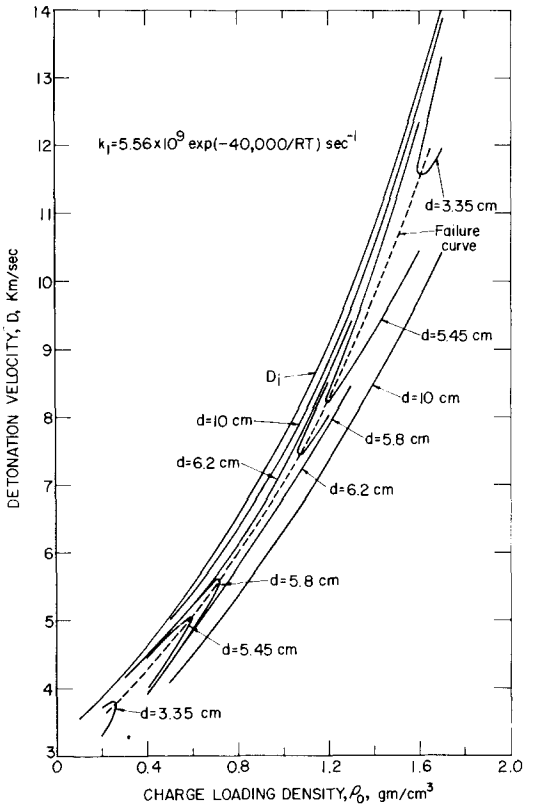

Fig. 2. Case 1: Two component porous granular explosive—variation of detonation velocity with loading density.

approaches D_i with increasing d at constant ρ_0) should represent "normal" non-ideal steady-state detonations. The physical reality of the lower velocity regime (D moving away from D_i with increasing d at constant ρ_0) is unclear at this time, but it does allow for the possible existence of a Chapman–Jouguet Low Velocity Detonation (LVD). Since the failure point is believed to be a discontinuity in the $dD/d\rho_0$ curve, a change from one detonation regime to another can not occur except by some jump mechanism. This factor would be consistent with those few observations which have been reported for LVD in granular explosives†.

Some time ago, Price (1967) observed that solid explosives could be classified into two groups based upon their detonation characteristics. Group I type explosives (e.g. PETN, TNT, RDX) exhibit critical diameters which *decrease* with increasing density, and detonation velocities at a given d which approach the ideal velocity with *increasing* density. This contrasts with the behavior of Group II type explosives (e.g. HN, NQ, AP) which exhibit the opposite effects, viz. critical

†see Taylor (1952), Cook (1958), Johansson and Persson (1970), Babaitsev *et al.* (1970) and Brown and Collins (1967).

diameters which *increase* with increasing ρ_0, and detonation velocities at a given d which approach the ideal velocity in the limit of *decreasing* ρ_0.

In Fig. 3 we have plotted the calculated d_{cr} vs ρ_0 for our sample explosive (depicted as the coarse grain curve). It is readily seen from this figure as well as from the velocity/density curves in Fig. 2, that the "normal" detonation, i.e. the high velocity regime, exhibits Group I characteristics for $\rho_0 > \sim 0.9\,g/cm^3$ and Group II characteristics for $\rho < \sim 0.9\,g/cm^3$. Indeed, Bobolev† has reported exactly such mixed behavior for 50/50 amatol mixtures. His reported curve is shown in Fig. 4. The curves marked theoretical are our attempts to calculate this particular case and will be discussed later on in greater detail.

The curve in Fig. 3 labeled fine grain shows the effect of decreasing the site dimensions L_1 and L_2 by a factor of 4. It is seen that decreasing the particle grain size has opposite effects on the Group I and Group II type explosive behavior, i.e. increasing d_{cr} in the former case and decreasing d_{cr} in the latter case. This critical

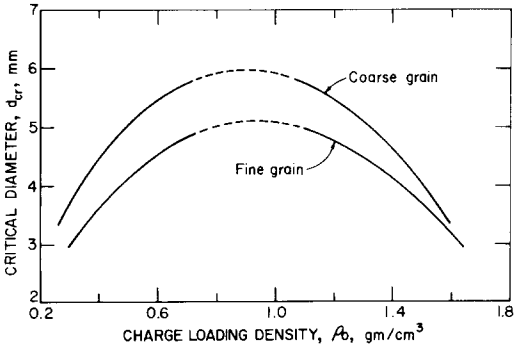

Fig. 3. Case 1: Two component porous granular explosive—variation of critical diameter with loading density. Coarse grain, $L_1 = L_2 = 50\ \mu m$; fine grain, $L_1 = L_2 = 12.5\ \mu m$.

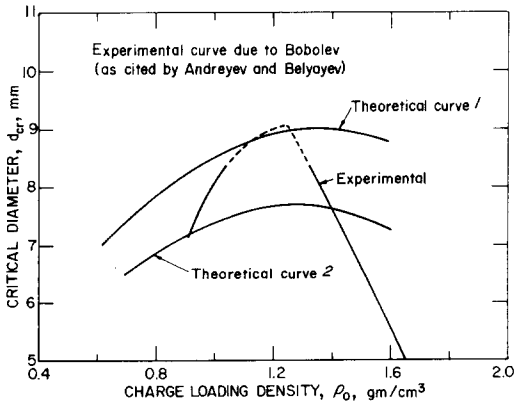

Fig. 4. Variation of critical diameter with loading density for ammatol (50/50).

†As cited by Andreyev and Belyayev (1960).

diameter behavior with particle size was another one of the contrasting patterns observed by Price (1967).

In Figs. 5 and 6 we depict the effects of a change in the pre-exponential factor, A_1 and A_s on the calculated detonation velocities. A decrease in the rate of decomposition of the solid by a factor of 100 increases d_{cr} (Fig. 5), but also extends the range of Group II behavior to higher densities. That is, increasing the grain-burning contribution to the detonation reaction time relative to that of the bulk decomposition reaction apparently enhances the Group II behavior. On the other hand, it is seen from Fig. 6 that Group I behavior is favored by increasing the relative importance of the bulk decomposition mechanism. While not totally unexpected, these results do clarify the effects that competing grain-burning and bulk decomposition reactions can have on the detonation velocity and the critical diameter.

An interesting aspect of Fig. 5 relative to Fig. 2 is the noticeable downward curvature of the high velocity regime D vs ρ_0 curve for $d = 71$ cm prior to intercepting the failure point at $\rho_0 \cong 0.8$. This is another characteristic of Group II explosives which was pointed out by Price (1967), and shown specifically for the case of ammonium perchlorate, a relatively low energy explosive material.

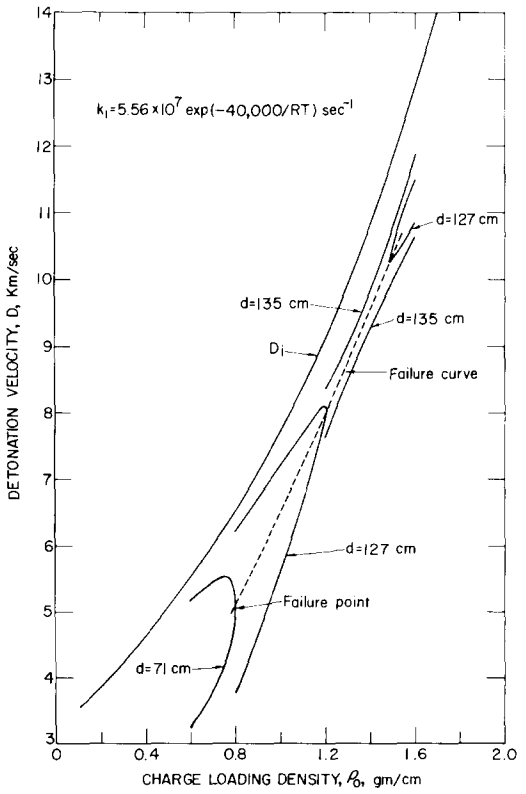

Fig. 5. Case 1: Two component porous granular explosive—effect of a decrease in bulk decomposition rate on detonation velocity.

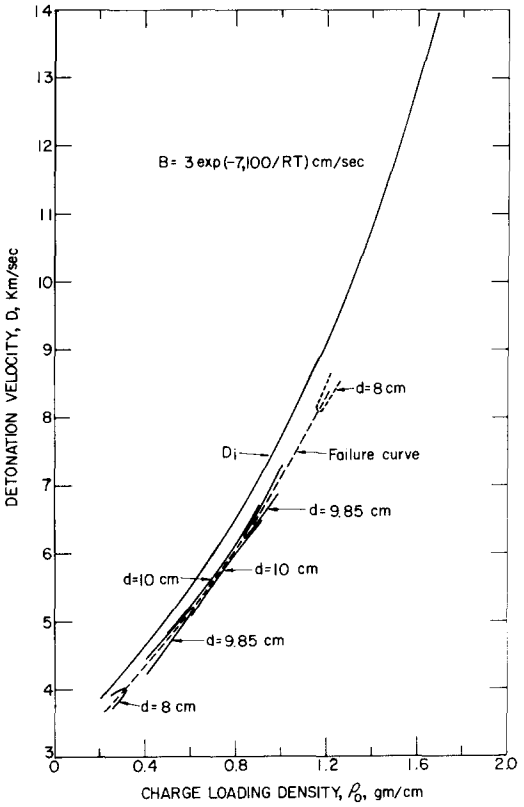

Fig. 6. Case 1: Two component porous granular explosive—effect of a decrease in grain burning rate on detonation velocity.

It appears from these results that the lattice model offers a realistic approach to describing heterogeneous explosive detonation phenomena.

Case 2. A three-component porous granular explosive

In this example, an attempt is made to correlate Bobolev's reported critical diameter data for amatol (50/50) which is shown in Fig. 4. The lattice is constructed by assuming the amatol to be a physical mixture of equal weights of spherical particles of TNT ($i = 1$) and NH_4NO_3 ($i = 2$) with the air spaces forming a third type initiation site ($i = 3$). Application of eqns (26)–(28) to this construction leads to

$$N_1(0) = \frac{d}{\Delta} L_2^3 L_3^3 \rho_2(\rho_3 - \rho_0) \tag{31}$$

$$N_2(0) = \frac{d}{\Delta} L_1^3 L_3^3 \rho_1(\rho_3 - \rho_0) \tag{32}$$

$$N_3(0) = \frac{d}{\Delta} L_1^3 L_2^3 [\rho_2(\rho_0 - \rho_1) - \rho_1(\rho_0 - \rho_2)] \tag{33}$$

$$\Delta = L_1L_2L_3\{L_3^2(\rho_3 - \rho_0)(L_1^2\rho_1 + L_2^2\rho_2) - L_1^2L_2^2[\rho_1(\rho_2 - \rho_0) + \rho_2(\rho_1 - \rho_0)]\}. \quad (34)$$

Table 2 lists the required input parameters. The value of γ is determined from an ideal detonation velocity calculation which yields a reasonable D_i (5400 m/sec) at $\rho_0 = 1.4\,\text{g/cm}^3$. The value of the pre-exponential factor for NH_4NO_3 decomposition was adjusted (by about a factor of 100) to fit the experimental d_{cr} data at a single point ($d_{cr} = 0.77$ cm, $\rho_0 = 1.35\,\text{g/cm}^3$). The final results are depicted in Fig. 4 as theoretical curve I. The overall agreement with experiment is not quantitative, but the theoretical curve does show the transition between Group I/Group II behavior at $\rho = 1.2$ to $1.3\,\text{g/cm}^3$.

Table 2. Input parameters for Case 2 explosive

$\rho_1 = 1.654\,\text{g/cm}^3$	$C_v = 0.3\,\text{cal/g°K}$
$\rho_2 = 1.73\,\text{g/cm}^3$	$\gamma = 1.2$
$\rho_3 = 10^{-3}\,\text{g/cm}^3$	$(q_d)_i = 720\,\text{cal/g}$
$L_1 = L_2 = 2 \times 10^{-3}$ cm	$T_0 = 300°\text{K}$
$L_3 = 5 \times 10^{-3}$ cm	
(a) $k_1 = 4.55 \times 10^{11} \exp(-43{,}000/RT)\,\text{sec}^{-1}$	
(b) $k_2 = 2.51 \times 10^{10} \exp(-38{,}300/RT)\,\text{sec}^{-1}$	
(c) $k_2 = 1.49 \times 10^{10} \exp(-38{,}300/RT)\,\text{sec}^{-1}$	
$k_3 = 10^{10}\,\text{sec}^{-1}$	
(d) $B = 300 \exp(-7100/RT)$ cm/sec	

(a) Cook (1958) cites $k = 3 \times 10^9 T \exp(-43{,}400/RT)\,\text{sec}^{-1}$ for TNT.
(b) Theoretical curve I—see footnote (a) in Table 1.
(c) Theoretical curve II—see footnote (a) in Table 1.
(d) See footnote (b) in Table 1.

Predicated on the notion that Bobolev's experimental data might have been obtained with confined explosive charges, an attempt to examine this factor was made by utilizing Eyring's curved front theory for the diameter effect in cased charges (Eyring *et al.*, 1949). This was accomplished by replacing eqn (19) by the expression

$$\frac{D}{D_i} = 1 - \frac{8.68(a/d)^2}{W_c/W_e} \quad (35)$$

where W_c/W_e is the ratio of mass of casing to that of explosive within a volume element. For our purposes, W_c/W_e was taken as unity, and A_2 adjusted to fit a new experimental point ($d_{cr} = 0.9$ cm, $\rho_0 = 1.25\,\text{g/cm}^3$). The results of these new calculations are depicted as theoretical curve II in Fig. 4, where it is seen that the agreement with experiment is still primarily qualitative.

It is conceivable that better agreement between theory and experiment could be achieved with further modifications to the input parameters, but in view of the simplifications involved in the equations and the uncertainties in the input data, such an effort would not be too meaningful. On the other hand, the qualitative agreement that was achieved is possibly as good as can be expected at this time.

Case 3. RDX adulterated composite propellant

It has been observed in an extensive experimental study of the detonation of RDX adulterated composite propellants,† that the RDX drastically reduces the critical diameter of the propellant.‡ In this section we describe our attempt to apply the lattice model to these test data.

For purposes of lattice construction, the propellant was initially considered to consist of spherical propellant particles ($i = 1$) with dimensions and reaction kinetics predominated by that of the large particle AP component of the propellant.§ The RDX particles ($i = 2$) were taken as a second component. Equations (26) and (28) then define the initial number of initiating sites for any specified mass fraction of RDX. For convenience the difference in solid density between the propellant and the RDX was neglected, however, the ideal heat of detonation was taken to vary with RDX content, i.e.

$$(q_d)_i = (1 - f_{\mathrm{RDX}})q_{\mathrm{prop}} + f_{\mathrm{RDX}}q_{\mathrm{RDX}} \tag{36}$$

where q_{RDX} and q_{prop} are the ideal heats of detonation of the RDX and propellant (i.e. AP), respectively.

Table 3 lists the various input parameters for this initial case. Here, k_1 and B are approximately that which have been reported for AP, having been adjusted somewhat to yield an approximate fit to the experimental point at $f_{\mathrm{RDX}} = 0.0475$.

The first two columns in Table 4 compare the experimental and calculated results. While the agreement appears reasonable at large f_{RDX}, there appears to be an increasing discrepancy between the data at small f_{RDX}.

The third column in Table 4 shows how the calculated results are altered if one assumes the propellant to have an inherent porosity of 2 vol %. This porosity value is not unreasonable for the propellants described by Irwin *et al.* (1965).

Table 3. Input parameters for Case 3 explosive

$\rho_1 = \rho_2 = 1.6\ \mathrm{g/cm^3}$	$C_v = 0.3\ \mathrm{cal/g°K}$
$L_1 = 1.2 \times 10^{-2}\ \mathrm{cm}$	$q_{\mathrm{RDX}} = 1500\ \mathrm{cal/g}$
$L_2 = 3 \times 10^{-3}\ \mathrm{cm}$	$T_0 = 300°\mathrm{K}$
$\gamma = 1.2$	$q_{\mathrm{prop}} = 260\ \mathrm{cal/g}$
(a) $k_1 = 3.2 \times 10^{9} \exp(-29{,}000/RT)\ \mathrm{sec^{-1}}$	
(b) $k_2 = 3.2 \times 10^{18} \exp(-47{,}500/RT)\ \mathrm{sec^{-1}}$	
(c) $B = 6.2 \times 10^{4} \exp(-18{,}000/RT)\ \mathrm{sec^{-1}}$	

(a) Elwell *et al.* (1967) cites $k = 7.16 \times 10^{10} \exp(-28{,}600/RT)\ \mathrm{sec^{-1}}$ for AP propellant.

(b) Gross and Amster (1962) cites $k = 3.2 \times 10^{18} \exp(-47{,}500/RT)\ \mathrm{sec^{-1}}$ for RDX.

(c) Andersen and Chaiken (1961) cites $B = 31T \exp(-22{,}000/RT)$ cm/sec for AP.

†A conventional propellant composition containing 60–70 wt% ammonium perchlorate (AP), ~15 wt% aluminum and ~15 wt% rubber binder in which varying amounts of AP are replaced with RDX.

‡see Irwin *et al.* (1965) and Elwell *et al.* (1966; 1967).

§The propellant contained a bimodal distribution of AP with mean diameters at 120 and 12 μm. The RDX particles were ~30 μm in diameter.

Table 4. Comparison of critical diameter data for RDX adulterated propellant

		d_{cr} (cm)		
f_{RDX}	(a) Expt'l.	Calc. (No Porosity)	Calc. (2% Porosity)	
0.092	6.8	8.4	7.4	
0.071	13.3	—	—	
0.0475	28.6	28.6	23.6	
0.021	59.7	77	—	
0.00375	122	182	119	
0 (b)	152 No-Go 183 Go	226	142	

(a) Elwell *et al.* (1967).
(b) Single test at each diameter.

Entrainment of small air spaces in the propellant would contribute to the porosity, and act as additional initiation sites ($i = 3$). For the purpose of this calculation, we considered eqns (26) and (28) with three types of sites, taking for the air sites $L_3 = 3 \times 10^{-3}$ cm, $\rho_3 = 1.2 \times 10^{-3}$ g/cm^3 and $k_3 = 10^{10}$ sec^{-1}. We see from Table 4 that this approach leads to considerable improvement in the agreement between theory and experiment. In fact, the agreement is rather remarkable in view of the uncertainties in the input parameters. It is noted that the Project SOPHY investigators applied a similar approach in correlating their d_{cr} data.

Some additional comparisons between the experimental data and those calculated for the 2 vol % porosity case are shown in Table 5. Here we list the available data on detonation velocity and detonation reaction time at d_{cr}. While the agreement is not as close as the well defined d_{cr} data, it is believed to be sufficient to support our lattice model approach.

Conclusions

It would appear that the lattice model expression for the detonation reaction in granular explosives offers a good prescription for evaluating the effect of

Table 5. Comparison of some detonation parameters for RDX adulterated propellant

	D_i (m/sec)		D_{cr} (m/sec)		τ_{cr} (μsec)	
f_{RDX}	Expt'l.	Calc.	Expt'l.	Calc.	Expt'l.	Calc.
(a) 0.092	4880	4730	4350	4370	<30	1.6
(b) 0.0475	—	4440	3960	4130	—	5.1
(b) 0.00375	—	4140	3800	3900	—	22
(c) 0	—	4110	3200	3890	—	25

(a) Experimental estimates from Elwell *et al.* (1966).
(b) Experimental estimates from Elwell *et al.* (1967).
(c) D_{cr} value is the velocity measured with a single charge of 183 cm diameter.

competing bulk decomposition and grain-burning reactions on detonability. The fact that Price's Group I/Group II contrasting explosives' behavior is a natural consequence of coupling the lattice model to Eyring Failure Theory is considered to be significant support for the validity of the approach taken. The application of the model for determining *a priori* the critical diameter of any given explosive mixture involves too many unknown kinetic parameters to yield quantitative results at this time. However, a good qualitative description of the variation of d_{cr} with varying ρ_0 appears reasonable.

The finding in this work of two Chapman–Jouguet detonation velocities for any given $d > d_{cr}$ has been noted by other investigators who have utilized Eyring Failure Theory. The possible existence of both a high and low velocity regime for Chapman–Jouguet detonations should take on added significance in view of the relatively recent accepted observations of LVD phenomena in granular explosives. However, at this time, there is insufficient evidence to warrant identification of our theoretical results with such experimental phenomena.

References

Andersen, W. H. and Chaiken, R. F. (1959) Application of surface decomposition kinetics to detonation of ammonium nitrate, *ARS J.* **29**, 49–51.

Andersen, W. H. and Chaiken, R. F. (1961) Detonability of solid composite propellants, *ARS J.* **31**, 1379–1387.

Andreyev, K. K. and Belyayev, A. F. (1960) *Theory of Explosive Substances.* Moscow; English translation AD643-597 Foreign Technology Division WP-AFB, Ohio. (Oct. 1966), p. 296.

Babaitsev, L. V., Kondrikov, B. N. and Tyshevich, V. F. (1970) *Low Velocity Detonation of Cast Explosive Charges* (Edited by B. D. Rossi), Vzryvnoe Delo Collection No. 68/25 (Moscow), pp. 194–201; Israel Program for Scientific Translations TT70-50163 (1971), available from U.S. Department of Commerce.

Brown, J. A. and Collins, M. (1967) *Explosion phenomena intermediate between deflagration and detonation*, Army Research Office STAF Report. Defense Documentation Center, Cameron Station, Alexandria, Va.

Cook, M. A. (1958) *The Science of High Explosives.* Reinhold, New York.

Elwell, R. B., Irwin, O. R. and Vail, Jr., R. W. (1966) *Project SOPHY—Solid Propellant Hazards Program.* Technical Documentary Report AFRPL-TR-66-25.

Elwell, R. B., Irwin, O. R. and Vail, Jr., R. W. (1967) *Project SOPHY—Solid Propellant Hazards Program.* Technical Report AFRPL-TR-67-211, Vol. I.

Evans, M. W. (1962) Detonation sensitivity and failure diameter in homogeneous condensed materials, *J. Chem. Phys.* **36**, 193–200.

Eyring, H., Powell, R. E., Duffey, G. H. and Parlin, R. B. (1949) The stability of detonation, *Chem. Rev.* **45**, 69–181.

Gross, D. and Amster, A. B. (1962) Thermal explosions: adiabatic self-heating of explosives and propellants, In *Eighth Symposium (International) on Combustion*, pp. 728–734. Williams and Wilkins, Baltimore.

Irwin, O. R., Roark, G. L. and Salzman, P. K. (1965) *Large solid-propellant boosters explosive hazards study program (Project SOPHY).* Technical Documentary Report AFRPL-TR-65-211. NTIS AD476617.

Johansson, C. H. and Persson, P. A. (1970) *Detonics of High Explosives.* Academic Press, New York.

Mader, C. L. (1965) *A study of the one-dimensional time-dependent reaction zone of nitromethane and liquid TNT.* Los Alamos Scientific Laboratory Report LA-3297.

Petrone, F. J. (1966) Validity of the classical detonation wave structure for condensed explosives, *Phys. of Fluids* **11**, 1473–1478.

Price, D. (1967) Contrasting patterns in the behavior of high explosives, In *Eleventh Symposium (International) on Combustion*, pp. 693–701. The Combustion Institute, Pittsburgh, Penn.

Taylor, J. (1952) *Detonation in Condensed Explosives.* Oxford at the Clarendon Press, London.